Pergamon

J. Quant. Spectrosc. Radiat. Transfer Vol. 59, No. 1/2, pp. 77–89, 1998

Printed in Great Britain
PII: S0022-4073(97)00135-0
0022-4073/98 $19.00 + 0.00

SOLUTION OF THE INVERSE PROBLEM OF RADIATIVE TRANSFER ON THE BASIS OF MEASURED INTERNAL FLUXES

N. FUKSHANSKY-KAZARINOVA†, L. FUKSHANSKY†‡§, M. KÜHL† and B. B. JØRGENSEN†

†Max-Planck-Institute for Marine Microbiology, Microsensor Research Group, Celsiusstr. 1, D-28359, Bremen, Germany and ‡Department of Biology, University of Freiburg, Schänzlestr. 1, D-79104, Freiburg, Germany

(Received 14 February 1997)

Abstract—A method for the solution of the inverse problem of radiative transfer is presented which utilizes the internal fluxes measured at different depths and in different directions with optical radiance microprobes in dense multiple scattering media. The method yields optical cross-sections and the phase function for the sample even when these parameters are depth dependent. The sensitivity analysis shows that the theoretical errors caused by the finite number of measurements as well as by the non-uniform directional sensitivity of the microprobes can be held on a low level; even the fourth Legendre coefficient of the unknown phase function can be recovered to the accuracy of 10%. Copyright © 1998 Elsevier Science Ltd. All rights reserved

Keywords—radiative transfer, inverse problem, radiance distributions in multiple scattering media, microsensor measurements, estimation of the optical parameters

1. INTRODUCTION

The inverse problem of radiative transfer—to find the optical parameters on the basis of available measurements of radiances and fluxes—is a central topic for many applied areas. Specifically in biomedical and ecological research this problem has recently attracted great attention because it opens way for modeling and general analysis of light-driven processes like photosynthesis without limitations imposed by the specific features of individual samples. Attempts to solve the inverse problem in biomedical optics[1–8] use different methods ranging from the adding–doubling method to the inverse Monte-Carlo technique and are restricted either to diffusion or to multi-flux approximation. To our knowledge, the full problem including the estimation of the unknown phase function was in no case approached on the level of the general equation of radiative transfer.

At the same time the experimental methods providing the input data for the theory improved strongly during the last years. One of these advancements is the three-dimensional measurement of the internal fluxes with the optical radiance microprobes increasingly employed in plant tissues, aquatic sediments, microbial mats and so called phantom media which provide optical models for medical applications.[9–15] Until recently this method was not applicable for quantitative analysis because of the so called instrumental error, an inherent undetermined inaccuracy which originates from the non-uniform directional sensitivity of the microprobe. However, since a novel theory of measurements provides a good correction for the instrumental error[16,17] the idea to develop a theory solving the complete inverse problem on the basis of this impressive data set has become reasonable and promising.

This is the aim of the present paper. The problem is formulated as follows. We consider a plane parallel turbid sample (Fig. 1) illuminated by a collimated light flux. Three-dimensional measurements of the internal fluxes are performed by the optical radiance microprobe at different

§Corresponding author Fax: + 49-761-203-2612; e-mail: lefu@ruf.uni-freiburg.de

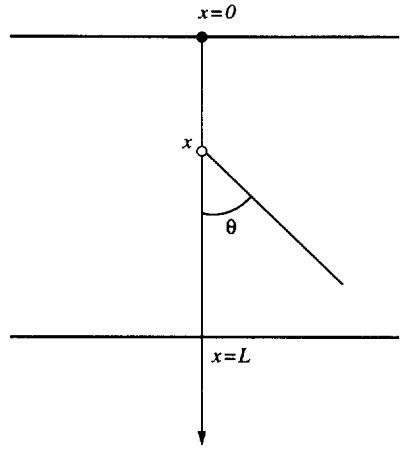

Fig. 1. Plan—parallel turbid sample of thickness L illuminated by a collimated flux F_0. x—depth coordinate; θ—zenithal angular coordinate.

depths, x_i and in different zenithal directions θ_j. The task is to obtain on the basis of these measurements the optical parameters, which can also depend on x: the extinction cross-section σ and the phase function $p(\mu,\mu')$, $(\mu = \cos\theta)$.

In Sec. 2.1 the theory is presented. It is based on the determination of subsequent moments of the radiance distribution using the equation of radiative transfer in which both the phase function and the directional cosine, μ, are developed into series of Legendre polynomials. The derivation results in a set of differential equations for the moments; these equations contain the Legendre coefficients of the phase function. Sec. 2.2 combines these results with the theory correcting the three-dimensional measurements for the instrumental error. It results in a set of differential equations which can be solved with respect to the Legendre coefficients of the phase function. In Sec. 2.3 containing an extended example of application we study the accuracy of the method and its stability under variable geometry of measurements and variable step size along the depth coordinate. Sec. 3 contains the concluding discussion and outlook.

2. RESULTS

2.1. Theory: the method of moments

We consider a plane parallel sample (Fig. 1) under collimated incident light flux F_0. The diffuse component of radiance $I(\tau,\mu)$ obeys the equation of radiative transfer

$$\mu \cdot \frac{\partial I(\tau,\mu)}{\partial \tau} + I(\tau,\mu) = 1/2 \int_{-1}^{1} I(\tau,\mu') \cdot p(\mu,\mu',x) \mathrm{d}\mu' + \frac{F_0}{4\pi} \cdot p(\mu,1,x) \cdot \mathrm{e}^{-\tau} \tag{1}$$

Here $p(\mu,\mu',x)$ is the phase function, $\mu = \cos\theta$, θ is the zenithal angle (cf., Fig. 1), $\tau = \sigma(x) \cdot x$ is the optical depth, $\sigma(x)$ is the extinction cross-section, and x is the vertical depth coordinate (cf., Fig. 1). Eq. (1) is written for a medium with azimuthal symmetry, i.e., I, p, σ are magnitudes integrated with respect to the azimuthal coordinate (cf. chapter 7 in Ref. [18]). Note that the optical parameters σ and p may vary with x.

Let us introduce the moments of the radiance distribution

$$K_n(\tau) = \int_{-1}^{1} \mu^n I(\tau,\mu) \mathrm{d}\mu; \qquad n = 0, 1, 2, \ldots . \tag{2}$$

The two first moments have a clear physical meaning: $K_0(\tau)$ is proportional to the total fluence rate of the diffuse radiant energy, $K_1(\tau)$ is proportional to downstream diffuse radiant flux.

As well known the phase function can be developed into series of Legendre polynomials[18]

$$p(\mu,\mu',x) = \sum_{i=0}^{\infty}(2i+1)\omega_i(x)P_i(\mu)P_i(\mu'), \tag{3}$$

specifically

$$p(\mu,1,x) = \sum_{i=0}^{\infty}(2i+1)\omega_i(x)P_i(\mu), \text{ since } P_i(1) = 1,\ i = 0, 1, 2, \ldots.$$

Our purpose in this section will be to establish relationships between the unknown Legendre coefficients ω_i of the phase function on the one hand and the moments K_n and their derivatives, which can be estimated from the measured internal fluxes, on the other hand.

Integrating over μ from -1 to 1 Eq. (1) multiplied by μ^n and using (2) and (3) we obtain

$$\frac{\partial K_{n+1}(\tau)}{\partial\tau} + K_n(\tau) = \sum_{i=0}^{\infty}(2i+1)\omega_i(x)\int_{-1}^{1}P_i(\mu)\mu^n d\mu\left[\frac{1}{2}\int_{-1}^{1}P_i(\mu')I(\tau,\mu')d\mu' + \frac{F_0}{4\pi}\cdot e^{-\tau}\right]. \tag{4}$$

The adding up in (4) continues only till $i = n$ since

$$\int_{-1}^{1}\mu^n P_i(\mu)d\mu = 0 \text{ for } i > n.$$

Let us consider the integrals in (4). We start with

$$\int_{-1}^{1}\mu^n P_i(\mu)d\mu \text{ for } i \le n.$$

Developing μ^n into series of Legendre polynomials[19]

$$\mu^n = \sum_{k=0}^{n}a_{nk}P_k(\mu),$$

$$a_{nk} = \begin{cases} \dfrac{(2k+1)n!!(n-1)!!}{(n+k+1)!!(n-k)!!} & \text{for the even } n+k \\ 0 & \text{for the odd } n+k, \end{cases}$$

we get

$$\int_{-1}^{1}\mu^n P_i(\mu)d\mu = \sum_{k=0}^{n}a_{nk}\int_{-1}^{1}P_k(\mu)P_i(\mu)d\mu = \frac{2}{2i+1}\cdot a_{ni}$$

$$\text{since } \int_{-1}^{1}P_k(\mu)P_i(\mu)d\mu = \begin{cases} \dfrac{2}{2i+1} & \text{for } i = k \\ 0 & \text{for } i \ne k. \end{cases}$$

Now we turn to the integral

$$\int_{-1}^{1}P_i(\mu)I(\tau,\mu)d\mu.$$

Since $P_i(\mu)$ is a polynomial of degree i[19]

$$P_i(\mu) = \sum_{k=0}^{i} b_{ik}\mu^k \text{ with}$$

$$b_{ik} = \begin{cases} (-1)^{(i-k)/2} \dfrac{(i+k)!}{2^i\left(\dfrac{i-k}{2}\right)!k!\left(\dfrac{i+k}{2}\right)!} & \text{for the even } i+k \\ 0 & \text{for the odd } i+k, \end{cases}$$

we obtain

$$\int_{-1}^{1} P_i(\mu)I(\tau,\mu)\mathrm{d}\mu = \sum_{k=0}^{i} b_{ik}\int_{-1}^{1} \mu^k I(\tau,\mu)\mathrm{d}\mu = \sum_{k=0}^{i} b_{ik}K_k(\tau)$$

Thus the formula (4) can be transformed to

$$\frac{\partial K_{n+1}(\tau)}{\partial\tau} + K_n(\tau) = \sum_{i=0}^{n} a_{ni}\omega_i(x)\sum_{k=0}^{i} b_{ik}K_k(\tau) + \frac{F_0 e^{-\tau}}{2\pi}\sum_{i=0}^{n}\omega_i(x)a_{ni}, \qquad n = 0,1,\ldots . \tag{5}$$

Below we give the explicit expressions of Eq. (5) for the first five values of n:

$$\frac{\partial K_1(\tau)}{\partial\tau} = -(1-\omega_0)K_0 + \frac{F_0 e^{-\tau}}{2\pi}\omega_0 \tag{6}$$

$$\frac{\partial K_2(\tau)}{\partial\tau} = -(1-\omega_1)K_1 + \frac{F_0 e^{-\tau}}{2\pi}\omega_1$$

$$\frac{\partial K_3(\tau)}{\partial\tau} = -(1-\omega_2)K_2 + K_0(\omega_0-\omega_2)/3 + \frac{F_0 e^{-\tau}}{2\pi}(\omega_0+2\omega_2)/3$$

$$\frac{\partial K_4(\tau)}{\partial\tau} = -(1-\omega_3)K_3 + 3K_1(\omega_1-\omega_3)/5 + \frac{F_0 e^{-\tau}}{2\pi}(3\omega_1+2\omega_3)/5$$

$$\frac{\partial K_5(\tau)}{\partial\tau} = -(1-\omega_4)K_4 + 6K_2(\omega_2-\omega_4)/7 + K_0(\omega_0/5 - 2\omega_2/7 +$$

$$3\omega_4/35) + \frac{F_0 e^{-\tau}}{2\pi}(\omega_0/5 + 4\omega_2/7 + 8\omega_4/35)$$

Summarizing the above derivations we arrive at the following conclusion. If at some depth x a set of moments K_n and their derivatives is estimated and also the cross-section σ is known then the corresponding number of Legendre coefficients ω_i can be calculated from the Eq. (5) or Eq. (6). The next step is to show how the moments and their derivatives can be obtained from the internal fluxes measured with optical microprobes.

2.2. Combining the method of moments with the measurements of internal fluxes

This section is essentially based on the theory of three-dimensional measurements with radiance microprobes and correction of these measurements for the specific instrumental error.[16,17] Below follows a summary of these results. A radiance microprobe directionally sensing light within a rather narrow acceptance angle can be advanced in any zenithal direction θ_i to any depth of a horizontal sample (c.f., Fig. 1). Imagine a unit sphere circumscribing point P at a depth x where these measurements are performed (Fig. 2). Subdivide the sphere into N horizontal spherical bands, the band i confined between the horizontal circles on the sphere having coordinates $\bar{\theta}_{i-1}$ and $\bar{\theta}_i$. To each band corresponds a single measurement in a direction θ_i ($\bar{\theta}_{i-1} \le \theta_i \le \bar{\theta}_i$). Figure 2 shows the vertical projection of the unit sphere with the first band concentrated to a point $\theta_1 = \bar{\theta}_1 = 0$

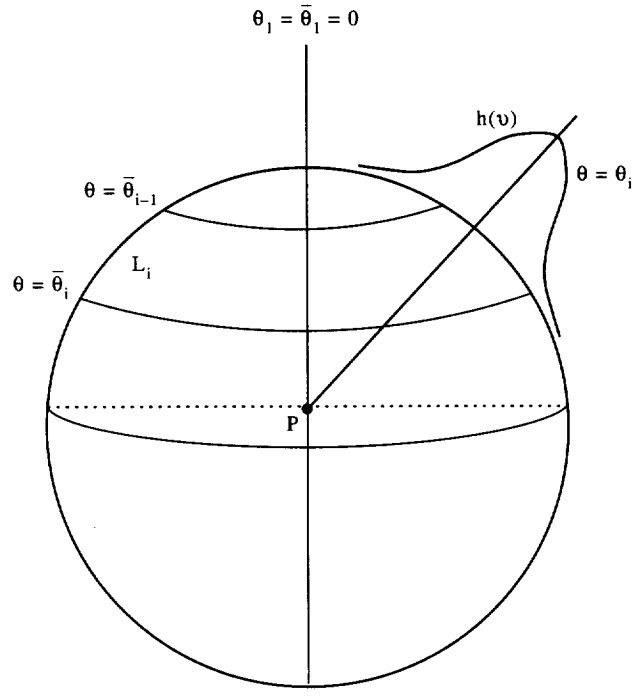

Fig. 2. Geometry of measurements with the radiance microprobes. The unit sphere is subdivided into N spherical bands, the first band is concentrated to a point. $\bar{\theta}_{i-1}, \bar{\theta}_i$—zenithal coordinates confining the band i. $\theta_i(\bar{\theta}_{i-1} \le \theta_i \le \bar{\theta}_i)$—direction of the measurement targeting the band i. L_i—the unknown radiance assumed to be constant over the band i. $h(\upsilon)$—the function of directional sensitivity of the microprobe; υ—angular deviation from the axis of the microprobe, $\upsilon = \theta - \theta_i$.

and corresponding to the collimated component of the radiation $L_1 = F_0 e^{-\sigma x}\delta(\mu - 1)$, where the δ-function obeys $\int_{-1}^{1}\delta(\mu)d\mu = 1$.

In this scheme the radiance distribution $I(x,\mu)$ is assumed to be a stepwise constant function having value L_i in a band number i. To the accuracy of this discretion the set of measured fluxes M_i ($i = 1, 2.., N$) is supposed to be an estimate of the radiance distribution $\{L_i\}$ and the radiant fluence rate (the scalar irradiance) appears as a sum of L_i's weighted with the fractional areas of the corresponding spherical bands on the unit sphere. However, a strong discrepancy between the sets $\{M_i\}$ and $\{L_i\}$—the instrumental error—arises due to the non-uniform directional sensitivity of the microprobe (see Fig. 2) which can be measured independently and presented as

$$h(\vartheta) = \cos\vartheta \cdot \exp(-m\sin^2\vartheta); \qquad \vartheta = \theta - \theta_i, \tag{7}$$

where m is the fitting parameter adjusting the function $h(\upsilon)$ to the individual curve of the microprobe under consideration. As seen in Fig. 2 the probe senses the incident radiation as weighted by the function $h(\upsilon)$ and also perceives contributions outside the targeted band. Hence, the sets $\{M_i\}$ and $\{L_i\}$ are connected by a system of linear equations

$$\sum_{j=1}^{n} J_{ij}L_j = M_i, \qquad i = 1, 2, \ldots, N, \tag{8}$$

where the coefficients J_{ij} are surface integrals of $h(\upsilon)$ with the domains of integration arising from the geometry of measurements, i.e., $\{\theta_i\}$ and $\{\bar{\theta}_j\}$. These integrals depend also on the probe parameter m. Specifically

$$J_{il} = \exp(-m\sin^2\theta_i)\cos\theta_i.$$

Thus the instrumental error can be eliminated by solving the system (8) with respect to L_i for any m and any geometry of measurements.

Now this result will be combined with the method of moments. From the measurements at different depths x_1, x_2.., x_M two sets of radiance values $L_i(x_j)$ are obtained:$\{x_j, L_1(x_j)\}$ $(j = 1.., M)$—for the collimated component $L_1(x) = F_0 e^{-\sigma(x)x}$and $\{x_j, L_i(x_j)\}$ $(j = 1.., M; i = 2.., N)$—for the diffuse component.

The first set is used to determine the extinction cross-section $\sigma(x)$. To this end assuming an integer $k \geq 1$ the fitting of M points $(x_j; \ln L_1(x_j))$ has to be performed by the polynomial of degree k

$$\ln L_1(x) \approx a_0 + a_1 x + a_2 x^2 + \ldots + a_k x^k.$$

The collimated component is presented then by the function

$$e^{a_0} \cdot \exp(a_1 + a_2 x + \ldots + a_k x^{k-1})$$

with $F_0 = e^{a_0}$ and $\sigma(x) = a_1 + a_2 x + ,. + a_k x_{k-1}$.

The second set provides the set of diffuse moments—$\{x_j, K_n(x_j)\}$—according to the formula

$$K_n(x_j) = \int_{-1}^{1} I(x,\mu)\mu^n dx = \sum_{i=2}^{N} \frac{L_i(x_j)}{n+1}\left(\cos^{n+1}\bar{\theta}_{i-1} - \cos^{n+1}\bar{\theta}_i\right) \tag{9}$$

which results in an obvious way from the discretion of the $I(x,\mu)$ and integration over each band. The set $\{x_j, K_n(x_j)\}$ is applied to determine the Legendre coefficients of the phase function. To this end Eq. (5) are discretized as follows. Consider the interval $[x_j, x_{j+1}]$. Designate its length as $\Delta x_j = x_{j+1} - x_j$ and its center as $\bar{x}_j = x_j + \Delta x_j/2$. The following approximations for terms of Eq. (6) in the point $\bar{x}_j$ are valid:

$$\frac{\partial K_n}{\partial \tau} \approx \frac{K_n(x_{j+1}) - K_n(x_j)}{\sigma(\bar{x}_j)\Delta x_j},$$

$$K_n \approx (K_n(x_{j+1}) + K_n(x_j))/2, \qquad e^{-\tau} = e^{-\sigma(\bar{x}_j)\bar{x}_j}.$$

With these approximations Eq. (5) can be solved with respect to $\omega_i(\bar{x}_j)$ $(i = 0, 1..; j = 1, 2.., M-1)$.

Thus a set of three-dimensional measurements with the radiance microprobes performed at different depths and corrected for the instrumental error provides the optical parameters of a sample. Now the questions concerning accuracy and stability of the method for variable geometry of measurements and parameter of the microprobe are of primary interest. In the next section an extended example of application will be used to perform sensitivity analysis and to answer these questions.

2.3. Example of application and sensitivity analysis

In this section we check the theory applying it to a sample with known optical properties. Solutions of the inverse problem for different values of the parameter of microprobe m and for different geometries of measurements are obtained providing a test for the stability of the method. The procedure includes following steps.

In Sec. 2.3.1 we find the radiance distributions at different depths of a sample with known (constant over the entire depth) σ and $P(\mu,\mu')$ and given incident flux F_0, i.e., solve the direct problem of radiative transfer. Sec. 2.3.2 treats the direct problem of measurements: we find how these radiance distributions are 'seen' by a microprobe at any direction θ_i (three different values of the microprobe parameter m are considered). Sec. 2.3.3 contains the application of the theory to these observable quantities M_i. Choosing a number of spherical bands which is reasonable for practical measurements, we compute for each band (on the basis of M_i and the band sizes) the values of L_i representing the constant radiance for each band. Then we apply these L_i values to solve the inverse problem with the method of moments. The optical parameters σ and ω_i (Legendre coefficients of $p(\mu,\mu')$) obtained in this way are compared to the corresponding magnitudes we started with in Sec. 2.3.1. The entire procedure is performed for three different geometries of measurements.

2.3.1. Solution of the equation of radiative transfer for a sample with known properties by the method of discrete ordinates. We consider a plane parallel turbid sample with thickness $L = 2$ units of length and extinction cross-section $\sigma = 2$ (unit of length)$^{-1}$ illuminated by collimated flux

$F_0 = 10$ unit of radiant flux normal to its surface. We assume that there are no jumps of refractive index at the sample boundaries, thus the boundary conditions for the diffuse component of radiation $I(x,\mu)$ are

$$I(0,\mu) = 0 \text{ for } \mu > 0 \qquad (10)$$

$$I(L,\mu) = 0 \text{ for } \mu < 0$$

As a phase function we take the Henyey–Greenstein function with the parameters $a = 0.8$ and $g = 0.5$. The development of this function into series of Legendre polynomials is

$$p(\mu,\mu') = a\sum_{i=0}^{\infty}(2i+1)g^i P_i(\mu)P_i(\mu'), \quad \text{i.e., } \omega_i = ag^i,\ i = 0, 1, \ldots.$$

To find the radiance distributions we solve Eq. (1) with the boundary conditions (10).

Solution was obtained with the discrete ordinates method (cf., chapter 8 in Ref. [20]). For the computation of the integrals of type

$$\int_{-1}^{1} f(\mu)\mathrm{d}\mu$$

the Gaussian quadrature formula was used. It is known[20] that the Gaussian quadrature

$$\sum_{i=1}^{M} w_i f(\mu_i)$$

provides best integration with the least number of quadrature points μ_i (and weights w_i). Specifically, an M points Gaussian quadrature will exactly integrate a polynomial of degree $2M - 1$.

We have used the standard Gaussian quadrature set for $M = 10$ as given in Table 1. For a discretion of Eq. (1) we introduce a spatial mesh

$$x_1 = 0, x_2, \ldots, x_{10} = L \quad \text{with } \Delta x = L/9.$$

Following specifications were made for the midpoint $\bar{x}_i = x_i + \Delta x/2$ of the ith mesh cell

$$\frac{\partial I(\bar{x}_i,\mu_j)}{\partial\tau} \approx \frac{I(x_{i+1},\mu_j) - I(x_i,\mu_j)}{\sigma\Delta x},$$

$$I(\bar{x}_i,\mu_j) \approx (I(x_{i+1},\mu_j) + I(x_i,\mu_j))/2, \qquad \mathrm{e}^{-\tau_i} = \mathrm{e}^{-\sigma\bar{x}_i}.$$

Table 1. Gaussian quadrature points used to solve the direct problem of radiative transfer with the method of discrete ordinates and further to simulate the result of measurements with corresponding geometry (Plan 2). i—number of a Gaussian point; θ_i (degrees)—zenithal coordinate; and w_i—the weight in the point i; $\mu_i = \cos\theta_i$.

i	w_i	μ_i	$\theta_i(^0)$
1	0.0667	0.9739	13.1
2	0.1494	0.8651	30.1
3	0.2191	0.6794	47.2
4	0.2693	0.4333	64.3
5	0.2955	0.1488	81.4
6	0.2955	−0.1488	98.6
7	0.2693	−0.4333	115.7
8	0.2191	−0.6794	132.8
9	0.1494	−0.8651	149.9
10	0.0667	−0.9739	166.9

Table 2. Solution of the direct problem of radiative transfer for the radiance values $I(x_i, \theta_j)$; x_i—depth; θ_j—Gaussian points. The second column corresponds to the collimated light $F_0 \cdot \exp(-\sigma x)$; $F_0 = 10$; $\sigma = 2$; L (thickness) = 2.

x	Values θ_i in degrees										
	0	13.1	30.1	47.2	64.3	81.4	98.6	115.7	132.8	149.9	166.9
0	10.000	0.000	0.000	0.000	0.000	0.000	0.594	0.559	0.495	0.445	0.416
2/9	6.412	1.102	0.787	0.596	0.576	0.820	0.668	0.556	0.468	0.408	0.377
4/9	4.111	1.572	1.148	0.881	0.799	0.743	0.611	0.492	0.404	0.347	0.318
6/9	2.636	1.681	1.249	0.960	0.819	0.684	0.534	0.418	0.336	0.284	0.258
8/9	1.690	1.603	1.208	0.926	0.755	0.593	0.450	0.344	0.270	0.224	0.201
10/9	1.084	1.437	1.095	0.837	0.658	0.498	0.369	0.274	0.208	0.169	0.150
12/9	0.695	1.239	0.954	0.726	0.555	0.408	0.295	0.209	0.151	0.119	0.104
14/9	0.446	1.041	0.808	0.611	0.456	0.326	0.226	0.146	0.097	0.073	0.063
16/9	0.286	0.858	0.670	0.503	0.367	0.254	0.176	0.077	0.045	0.032	0.027
$L = 2$	0.183	0.694	0.543	0.402	0.282	0.178	0.000	0.000	0.000	0.000	0.000

Designating $I(x_i,\mu_j) = \varphi_{ij}$ we arrived at the following approximation of Eq. (1):

$$\mu_j \frac{\varphi_{i+1,j} - \varphi_{i,j}}{\sigma \Delta x} + \frac{\varphi_{i+1,j} + \varphi_{ij}}{2} = \frac{1}{2} \sum_{k=1}^{10} p(\mu_j,\mu_k) w_k \frac{\varphi_{i+1,k} + \varphi_{i,k}}{2} + \frac{F_0}{4\pi} p(\mu_j,1) e^{-\sigma \bar{x}_i}, \qquad (i = 1,2,\ldots,9;\ j = 1,\ldots,10)$$

The set of 90 equations contains 100 unknown φ_{ij} ($i = 1..,\ 10; j = 1..,\ 10$). The boundary conditions at each boundary

$$\varphi_{1j} = 0, \qquad j = 1, ,.., 5;$$

$$\varphi_{10j} = 0, \qquad j = 6, ,.., 10;$$

provide the additional 10 equations to complete the set and allow for a solution. Results of the computation of the radiances $I(x_i,\mu_j)$ are presented in Table 2. The moments $K_n(x_i)$ were calculated on the basis of radiances also using the Gaussian quadrature

$$K_n(x_i) = \sum_{j=0}^{1} w_j I(x_i,\mu_j) \mu_j^n . \qquad (11)$$

Figure 3 shows the first four moments K_n ($n = 0,1,2,3$) as functions of depth x.

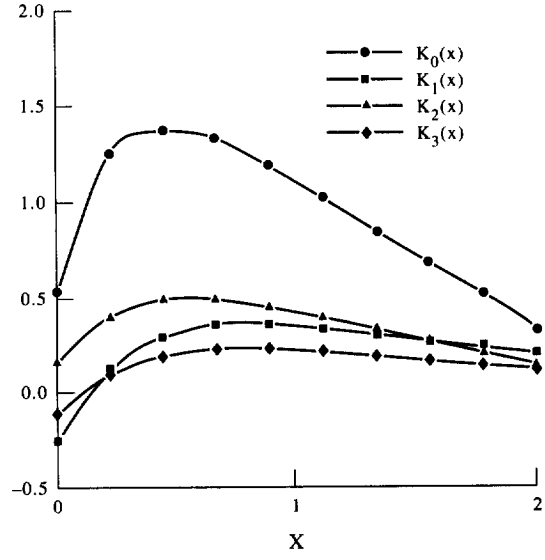

Fig. 3. The first four moments K_n ($n = 0,1,2,3$) obtained on the basis of the solution of the direct problem of radiative transfer given in Table 2. x—the depth coordinate; $L = 2$—thickness of the sample.

2.3.2. Determination of the radiant fluxes $M(\theta)$ observable by the optical microprobes. The diffuse component of radiance is determined for 10 directions at each of 10 depth x_i (see Table 2). For any fixed depth we obtain on the basis of Table 2 the diffuse radiance as a continuous function of θ: $I(x,\theta)$. Now using Eq. (8) in a direct way, i.e., calculating M_i we can estimate how this radiance distribution will be seen by a microprobe at any direction θ_i. For this purpose we discretize $I(x,\theta)$ subdividing the unit sphere into 36 bands of size 5^0. The constant within a band value of the diffuse radiance $L_j(x)$ is obtained as the value of $I(x,\theta)$ in the 5^0-band center:

$$L_j(x) = I(x,\theta_j), \quad \theta_j = 5(j-1) - 2.5(^0), \quad j = 2, \ldots, 36.$$

The collimated component is determined as

$$L_1(x) = F_0 e^{-\sigma x}$$

For any depth x and any assumed parameter of the microprobe m the observable magnitude $M_i(x) = M(x,\theta_i)$ can now be calculated from Eq. (8). Results of these calculations are given in Fig. 4 for four different depths x and three different values of the probe parameter

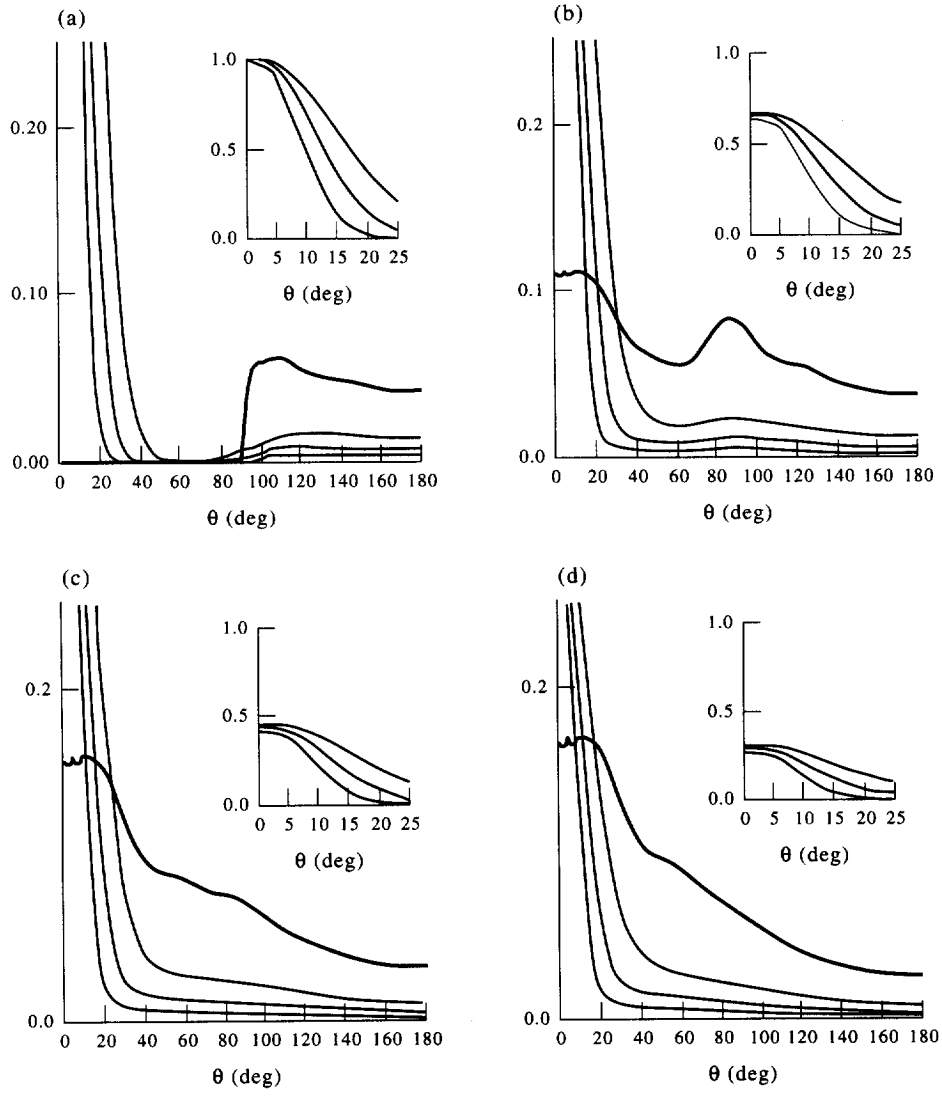

Fig. 4. Observable fluxes $M(\theta)/F_0$ (thin curves) calculated for 3 values of the probe parameter m (curves from the left to the right correspond to m values 40, 20, 10) on the basis of the radiance distribution $L(\theta)/F_0$ (thick curve). Abscissa–zenithal coordinate θ in degrees. Insets show the curves $M(\theta)$ in the range of small θ on large scale. Plates (a)–(d) show calculations performed for the depths $x = 0$; $x = 2/9$; $x = 4/9$; $x = 6/9$ respectively.

$m = 40,20,10$. The variation of m values can be made visible by expressing m in terms of another parameter—the acceptance angle of the probe α—which is the value $\upsilon_{1/2}$ providing 50% of the maximal sensitivity: $h(\upsilon_{1/2}) = 1/2$ (c.f., Eq. (7)). Specifically the values $m = 40,20,10$ used in the test correspond to $\alpha = 7{,}5^0$ (very peaked sensitivity function) $\alpha = 10{,}7^0$ (intermediate function), $\alpha = 15^0$ (very smooth sensitivity function) respectively. As seen in Fig. 4 the non-corrected measured quantity $M(\theta)$ (three thin curves for different m values) differs strongly from the real radiance distribution (thick curve) this discrepancy being larger for larger acceptance angles of the probe.

2.3.3. Solution of the inverse problem using the observable quantities corrected for the instrumental error. At this last step we will calculate the optical parameters of the sample on the basis of the observable magnitude $M(x, \theta)$. To this end we should choose the plan of measurements: a set of directions θ_j ($j = 1.., N$; $\theta_1 = 0$) of measurements and a subdivision of the unit sphere into a set of bands with assumed constant values of radiance. Then we should calculate for each depth x_i these constant values $L_j(x_i)$ on the basis of $M_j(x)$, i.e. correct for the instrumental error. Note that this correction will be made each time on the basis of a concrete chosen plane of measurements, e.g., with the corresponding band sizes. In conclusion we calculate on the basis of $L_j(x_i)$ the cross-section σ and the Legendre coefficients ω_i of the phase function with the method of moments. These results should be then compared to the initial true values we started with in Sec. 2.3.1.

The entire above procedure has been performed for three plans of measurements

1. Equidistant measurements with the step 20° ($N = 10$).
2. Measurements in the Gaussian points θ_j according to Table 1 with an additional measurement in the point $\theta = 0$ ($N = 11$). In this case the moments have been calculated according to Eq. (11).
3. Equidistant measurements with the step 10^0 ($N = 19$).

For each plan of measurements the subdivision of the sphere into bands is implied by the set θ_j; the coordinates $\bar{\theta}_j$ of the circles confining the bands are given as

$$\bar{\theta}_j = (\theta_{j+1} + \theta_j)/2 \qquad (j = 2, \ldots, M-1;\ \bar{\theta}_1 = 0).$$

Since it has been shown[16, 17] that from a given set $\{M_j\}$ the procedure correcting for the instrumental error recovers practically the same set $\{L_j\}$ independently of what probe parameter m has been applied the following calculations were restricted to single value $m = 20$.

Table 3 shows an example of intermediate results: the values $L_j(x_i)$ ($j = 1.., 11$; $i = 1.., 10$) for the plan 2 (compare to the data in Table 2). All the final results—the computed values of F_0, σ, ω_0, ω_1, ω_2, ω_3, ω_4 based on three different sets of measured data (plans 1–3) together with the true values of these magnitudes—are collected in Table 4. The ω_i values are averaged over all depth. For each ω_i three different step size along the depth coordinate were used when computing the increments of the moments according to Eq. (9). Calculations based on step sizes $L/9$ (using depths layers 1–2, 2–3..); $2L/9$ (using depths layers 1–3, 2–4..); $3L/9$ (using depths layers 1–4, 2–5..) are presented in the lines 1, 2 and 3 respectively.

Table 3. Solution for the plan 2 for the collimated (column 2) and diffuse radiance values $L_j(x_i)$ obtained from the observable fluxes $M(x_i, \theta_j)$ with the procedure correcting for instrumental error.

x	Values θ_i in degree										
	0	13.1	30.1	47.2	64.3	81.4	98.6	115.7	132.8	149.9	166.9
0	10.027	−0.189	0.037	−0.004	−0.011	0.046	0.885	0.648	0.486	0.468	0.416
2/9	6.422	1.016	0.808	0.572	0.588	0.802	0.743	0.566	0.500	0.417	0.383
4/9	4.119	1.516	1.159	0.864	0.810	0.724	0.672	0.515	0.427	0.359	0.322
6/9	2.640	1.655	1.254	0.948	0.829	0.662	0.598	0.438	0.358	0.295	0.261
8/9	1.692	1.593	1.210	0.918	0.762	0.571	0.509	0.364	0.289	0.234	0.204
10/9	1.085	1.433	1.097	0.831	0.664	0.478	0.423	0.291	0.226	0.178	0.152
12/9	0.695	1.240	0.955	0.721	0.558	0.391	0.343	0.225	0.164	0.126	0.106
14/9	0.445	1.046	0.808	0.608	0.458	0.312	0.268	0.161	0.109	0.078	0.063
16/9	0.286	0.862	0.671	0.502	0.367	0.242	0.215	0.096	0.046	0.038	0.026
2	0.187	0.653	0.508	0.360	0.257	0.100	0.013	−0.004	0.001	−0.000	0.000

Table 4. Values of the incident flux F_0, the extinction cross-section σ and Legendre coefficients of the phase function ω_i ($i = 0,..., 4$) recovered as solution of the inverse problem. In brackets the true values are given. Three experimental designs (plans 1–3) and three step sizes along the depth coordinate (lines 1–3) are used; in brackets, the relative error in per cent is presented. The calculated values are the averages over the entire depth of the sample

Calculated magnitude (its true value)		Plan 1: Equidistant with step 20°	Plan 2: Gaussian points with step 10°	Plan 3: Equidistant with step 10°
F_0 (10)		9.9380	10.0190	10.0010
σ (2)		1.9790	2.0006	2.0022
ω_0(0.8)	1	0.8030 (+0.4%)	0.8067 (+0.8%)	0.8033 (+0.4%)
	2	0.8049 (+0.6%)	0.8078 (+1.0%)	0.8051 (+0.6%)
	3	0.8062 (+1.0%)	0.8111 (+1.4%)	0.8084 (+1.0%)
ω_1(0.4)	1	0.3868 (−3.3%)	0.3896 (−2.6%)	0.3903 (−2.4%)
	2	0.3819 (−4.5%)	0.3845 (−3.9%)	0.3848 (−3.8%)
	3	0.3732 (−6.7%)	0.3756 (−6.1%)	0.3761 (−6.0%)
ω_2(0.2)	1	0.1864 (−6.8%)	0.1911 (−4.5%)	0.1965 (−1.7%)
	2	0.1871 (−6.5%)	0.1900 (−5.0%)	0.1961 (−1.9%)
	3	0.1853 (−7.3%)	0.1868 (−6.6%)	0.1946 (−2.7%)
ω_3(0.1)	1	0.1186 (+18.6%)	0.1252 (+25%)	0.1253 (+25.0%)
	2	0.1205 (+20.5%)	0.1311 (+31.0%)	0.1266 (+26.6%)
	3	0.1231 (+23.1%)	0.1335 (+33.5%)	0.1290 (+29.0%)
ω_4(0.05)	1	0.0432 (−13.6%)	0.0564 (+12.7%)	0.0424 (−15.2%)
	2	0.0395 (−20.9%)	0.0571 (+14.1%)	0.0444 (−11.0%)
	3	0.04092 (−18.2%)	0.0599 (+19.8%)	0.0482 (−3.7%)

As seen in Table 4 the values of F_0, σ are recovered with negligible errors, the errors for ω_0, ω_1, ω_2 are between 1% and 6%. Only for ω_3, ω_4 having small absolute values the errors reach in some cases 20%. As expected the error for a given ω_i increases with increasing distance between the neighboring depths involved in the estimation of the increments of moments (compare lines 1–3). Even more important error source is the flattening of the gradients of moments in the deep region of the sample (c.f., Fig. 4). The results averaged over the entire sample shown in Table 4 are heavily loaded with the large errors occurring in the lower half of the sample where the moment gradients become flat. The same results for ω_i as in Table 4 but averaged over the upper half where the curves $K_n(x)$ are steep show strongly decreased errors, so that also ω_3, ω_4 are determined to the accuracy of about 10% (Table 5). A comparison of different plans shows that measurements in Gaussian points (plan 2) are more accurate then the equivalent equidistant set (plan 1). Plan 3 produces the same accuracy as plan 2 but at the prize of a doubled number of measurements.

We can conclude that the theoretical errors caused by the inversion of the problem of radiative transfer and by the discretion of the radiance distribution due to finite number of measurements are rather small. Legendre coefficients up to ω_4 can be recovered with the error not exceeding 10%. The method is stable with respect to the variations of the geometry of measurements and of the step along the depth coordinate. A practical recommendation for increasing the accuracy is to repeat the measurements illuminating the opposite side or, if possible, to dissect the sample laterally. In both cases optical parameters at some depths can be studied then under condition of

Table 5. The same magnitudes as in Table 4, however the calculated values are averaged over the upper half of the sample where the gradient of the moments are steeper (c.f., Fig. 4). The relative errors are significantly lowered

Calculated magnitude (its true value)		Plan 1: Equidistant with step 20°	Plan 2: Gaussian points with step 20°	Plan 3: Equidistant 3 with step 10°
ω_0 (0.8)	1	0.7965 (−0.4%)	0.8064 (+0.8%)	0.7986 (−0.2%)
	2	0.7990 (−0.1%)	0.8059 (+0.6%)	0.8004 (+0.05%)
ω_1 (0.4)	1	0.3917 (−2.1%)	0.3939 (−1.5%)	0.3983 (−0.4%)
	2	0.3784 (−5.4%)	0.3805 (−4.9%)	0.3834 (−4.1%)
ω_2 (0.2)	1	0.1975 (−1.2%)	0.1938 (−3.1%)	0.2037 (+1.8%)
	2	0.1982 (−0.9%)	0.1952 (−2.4%)	0.2042 (+2.1%)
ω_3 (0.1)	1	0.1008 (+0.8%)	0.1124 (+12.4%)	0.1061 (+6.1%)
	2	0.1081 (+8.1%)	0.1184 (+18.4%)	0.1128 (+12.8%)
ω_4 (0.05)	1	0.0409 (−18.2%)	0.0548 (+9.5%)	0.0472 (−5.6%)
	2	0.0384 (−23.2%)	0.0517 (+3.4%)	0.0446 (−10.7%)

steeper curves $K_m(x)$ providing smaller error. It should be noted that in this example we had the constant over all depth σ and $p(\mu, \mu')$ to facilitate the sensitivity analysis. The method is, however, not restricted to constant parameters and yields the x-dependent magnitudes from different depths.

3. CONCLUDING REMARKS

Generally relations involving moments of the radiance distribution are convenient and some of them were used for theoretical and practical purposes. The first equation of the system (6) is nothing else as the continuity equation for the radiant flux in the x direction (cf., chapter 7.3 in Ref. [18]). It is reduced to a conservation law when no internal sources are present (i.e., $F_0 = 0$). In the hydro-optics this conservation law known as Gershun's law (cf. chapter 5.10 in Ref. [21]) was used to estimate on the basis of the measured $\Delta K_l/\Delta x$ and K_0 the absorption cross-section which is $\sigma\cdot(1 - \omega_0)$ in our designations. Morse and Feshbach[22] wrote explicitly two first Eq. (6) (with $F_0 = 0$) when discussing diffusion equation in their fundamental work (see chapter 12.2 in Ref. [22]). They noted that the equations for higher moments may have the standard structure of the two first equations, i.e., the derivative of a higher moment is a function of the previous moment and previous Legendre coefficient. This is not quite right as seen from Eq. (6), where the derivatives of the even moments depend on the all previous odd moments and Legendre coefficients and *vice versa*.

To our knowledge no attempts to apply the relationships between the moments and the phase function for a derivation of a general approach to inverse problem have been reported before and it is understandable: there was no reliable experimental basis for this application. Only the introduction of reproducible three-dimensional measurements of the internal fluxes together with the theory correcting for the instrumental error suggest this idea. The first step after deriving the theory (Sec. 2.3.1 and Sec. 2.3.2) was the sensitivity analysis and the estimation of the theoretical errors originated by the inversion and discretion of the problem of radiative transfer (Sec. 2.3.3). These universal errors should be separated from the experimental errors which depend on the nature of the sample and on the measuring device.

The next step (in progress) will be the experimental test where only one part of the measured data is theoretically processed while another part is compared to the radiance distributions calculated with the optical parameters obtained as solution of the inverse problem. Generally an additional random item arising in the measured magnitudes due to the experimental errors can, for some types of operators, cause a disproportionately large error in the solution of the inverse problem (so called improperly posed inverse problems[23, 24]). In such cases special treatments are necessary. Results obtained in Sec. 2.3.3 suggest, that this is a 'good' operator providing stable solutions also for varying input data. However, only after performing experimental tests and clarifying the above points the method presented in this paper may become a standard one for all cases where the measurements of the internal fluxes appear feasible.

Acknowledgements—This study was supported by grant Fu 152/6-2 from Deutsche Forschungsgemeinschaft, the Max-Planck Gesellschaft, and the Carlsberg foundation, Denmark (B.B. Jørgensen)

REFERENCES

1. Fukshansky, L., Fukshansky-Kazarinova, N. and Martinez v. Remisowsky, A. *Appl. Opt.*, 1991, **30,** 3145.
2. Prahl, S. A., van Gemert, M. C. and Welch, A. J., *Appl. Opt.*, 1993, **32,** 559.
3. Patterson, M. S., Chance, B. and Wilson, B., *Appl. Opt.*, 1989, **28,** 2331.
4. Groenhuis, R. A., Ferwerda, H. A. and Ten Bosch, J. J., *Appl. Opt.*, 1983, **22,** 2456.
5. Fukshansky, L., in *Photon-vegetation interactions: Applications in optical remote sensing and plant ecology*, ed. R. B. Myneni and J. Ross. Springer, Berlin, 1991, p. 253.
6. Bonner, R. A., Nossal, R., Havlin, S. and Weiss, G. H., *J. Opt. Soc. Am. A*, 1987, **4,** 423.
7. Steinke, J. M. and Shepherd, A. P., *IEEE Trans. Biomed. Eng. BME*, 1986, **34,** 826.
8. Farrell, T. J., Patterson, M. S. and Wilson, B. C., *Med. Phys.*, 1992, **19,** 879.
9. Vogelmann, T. C. and Björn, L. O., *Physiol. Plant.*, 1984, **60,** 361.
10. Vogelmann, T. C., Martin, G., Chen, G. and Buttry, D., *Adv. Bot. Res.*, 1991, **18,** 255.
11. Richter, T. and Fukshansky, L., *Photochem. Photobiol.*, 1996, **63,** 507.
12. Lilge, L., Haw, T. and Wilson, B. C., *Phys. Med. Biol.*, 1987, **38,** 215.
13. Jørgensen, B. B. and Des Marais, D. J., *Limnol. Oceanogr.*, 1986, **31,** 1376.
14. Kühl, M. and Jørgensen, B. B., *Limnol. Oceanogr.*, 1994, **39,** 1368.

15. Kühl, M., Lassen, C. and Jørgensen, B. B., in *Microbial mats: Structure, development and environmental significance*, ed. L. J. Stal and P. Gaumette. NATO ASI Series G, Springer, Berlin, 1994, p. 149.
16. Fukshansky-Kazarinova, N., Fukshansky, L., Kühl, M. and Jørgensen, B. B., *Appl. Opt.*, 1996, **35,** 65.
17. Fukshansky-Kazarinova, N., Fukshansky, L., Kühl, M. and Jørgensen, B. B., *Appl. Opt.*, 1997, **36,** 6520.
18. Ishimaru, A., *Wave Propagation and Scattering in Random Media*. Academic Press, New York, 1978.
19. Hobson, E. W., *The Theory of Spherical and Ellipsoidal Harmonics*. Cambridge University Press, Cambridge, 1931.
20. Duderstadt, J. J. and Martin, W. R., *Transport Theory*. John Wiley, New York, 1979.
21. Mobley, C. D., *Light and Water, Radiative Transfer in natural Waters*. Academic Press, San Diego, 1994.
22. Morse, P. M. and Feshbach, H., *Methods of Theoretical Physics*. McGraw Hill, New York, 1953.
23. Tikhonov, A. N. and Arsenin, W. J., *Methods of the Solution of Ill-posed Problems*, (in Russian). Nauka, Moscow, 1979.
24. Turchin, V. F., Kozlov, V. P. and Malkevich, M. S., *Usp. Fis. Nauk*, 1970, **102,** 345 in Russian.